Coarse-grain simulations of active molecular machines in lipid bilayers

Mu-Jie Huang, Raymond Kapral, Alexander S. Mikhailov, and Hsuan-Yi Chen

Citation: The Journal of Chemical Physics **138**, 195101 (2013); doi: 10.1063/1.4803507
View online: http://dx.doi.org/10.1063/1.4803507
View Table of Contents: http://scitation.aip.org/content/aip/journal/jcp/138/19?ver=pdfcov
Published by the AIP Publishing

Coarse-grain simulations of active molecular machines in lipid bilayers

Mu-Jie Huang,[1] Raymond Kapral,[2] Alexander S. Mikhailov,[3] and Hsuan-Yi Chen[1,4,5]
[1]*Department of Physics, National Central University, Jhongli 32001, Taiwan*
[2]*Chemical Physics Theory Group, Department of Chemistry, University of Toronto, Toronto, Ontario M5S 3H6, Canada*
[3]*Abteilung Physikalische Chemie, Fritz-Haber-Institut der Max-Planck-Gesellschaft, Faradayweg 4-6, 14195 Berlin, Germany*
[4]*Institute of Physics, Academia Sinica, Taipei 11520, Taiwan*
[5]*Physics Division, National Center for Theoretical Sciences, Hsinchu 30013, Taiwan*

(Received 6 February 2013; accepted 12 April 2013; published online 15 May 2013)

A coarse-grain method for simulations of the dynamics of active protein inclusions in lipid bilayers is described. It combines the previously proposed hybrid simulations of bilayers [M.-J. Huang, R. Kapral, A. S. Mikhailov, and H.-Y. Chen, J. Chem. Phys. **137**, 055101 (2012)], based on molecular dynamics for the lipids and multi-particle collision dynamics for the solvent, with an elastic-network description of active proteins. The method is implemented for a model molecular machine which performs active conformational motions induced by ligand binding and its release after reaction. The situation characteristic for peripheral membrane proteins is considered. Statistical investigations of the effects of single active or passive inclusions on the shape of the membrane are carried out. The results show that the peripheral machine produces asymmetric perturbations of the thickness of two leaflets of the membrane. It also produces a local saddle in the midplane height of the bilayer. Analysis of the power spectrum of the fluctuations of the membrane midplane shows that the conformational motion of the machine perturbs these membrane fluctuations. The hydrodynamic lipid flows induced by cyclic conformational changes in the machine are analyzed. It is shown that such flows are long-ranged and should provide an additional important mechanism for interactions between active inclusions in biological membranes. © *2013 AIP Publishing LLC*. [http://dx.doi.org/10.1063/1.4803507]

I. INTRODUCTION

More than half of all proteins interact with biomembranes and a significant fraction of the biomembrane mass in a cell is due to protein inclusions.[1] Membrane proteins carry out numerous functions. Structural proteins attached to the cytoskeleton are responsible for mechanical stability of biological cells, whereas adhesion proteins allow cells to recognize each other and to interact. Ion pumps and membrane channels are essential for transmembrane transport of particles. Receptors play an important role in intracellular signal transduction and membrane enzymes produce substances needed for cell operation. Bin-Amphiphysin-Rvs (BAR) domain proteins, which stabilize tubular membrane structures, play a role in membrane fission processes.[2,3] The proteins may span the entire membrane (for example, ion pumps) or may only be attached in one lipid monolayer (BAR domain proteins). While some of these functions are static in nature, many of them are dynamic and involve cyclic conformational changes, which require a continuous supply of energy. Dynamic membrane proteins are active inclusions and function as molecular machines.[4]

Due to coupling between the proteins and the lipid bilayer, conformational changes in active inclusions can significantly affect the membranes in which they reside. Experiments showing changes in membrane fluctuation behavior induced by active protein inclusions have been carried out.[5] Collective effects of active protein inclusions on membrane stability and dynamics have been investigated theoretically, but at a phenomenological level that does not resolve the detailed structures of the proteins and lipid bilayers.[6–10]

Membrane proteins have been studied using all-atom molecular dynamics (MD) simulations.[11,12] Since these systems comprise proteins, lipids, and water molecules, the MD simulations are computationally intensive and the dynamics of small systems could be followed for short times (typically, for a membrane with a linear size of about ten nanometers and over nanosecond time scales, see, e.g., Refs. 11 and 12). However, the characteristic timescales of cyclic conformational motions that underlie the activity of protein machines range from microseconds to tens of milliseconds; thus, full MD simulations of membranes with active inclusions over all relevant time scales are not currently feasible.

Various coarse-grain models of proteins have been constructed. In Go-like models, entire residues are replaced by single point particles interacting through effective pairwise potentials.[13] A further reduction in the description is made in elastic-network (EN) models[14–16] where the point particles are assumed to interact through elastic potential functions, and elastic networks are constructed using experimental X-ray diffraction data for actual proteins.[17–20] Despite their simplicity, EN models have been able to describe many features of protein dynamics; for instance, the thermal fluctuations (B factors) of various proteins (see, e.g., Ref. 21), conformational relaxation processes in proteins[17] and conformational responses to ligand binding or the application of external forces.[18,22] Such models have been extended to account for partial unfolding and refolding of proteins and used in a

study of the turnover cycles of the enzyme adenylate kinase.[23] The entire operation cycles of the molecular motor hepatitis C helicase, including its interactions with DNA, could be reproduced using an EN model.[18]

Several coarse-grain models for lipid membranes have been proposed and implemented. Single lipid molecules are often modeled as chains of molecular groups or beads that interact through effective potentials; lipid molecules within the membrane also interact through such effective potentials. A very simple solvent-free coarse-grain model for a lipid membrane, where individual lipids are modeled by three beads connected by elastic interactions, was constructed by Cooke *et al.*[24] Other models explicitly include solvent, albeit at a coarse-grain level.[25,26] The dynamics of the lipid membrane may then be followed using molecular dynamics, but for a system with fewer particles than in a full atomistic model. A higher level of coarse graining is provided by dissipative particle dynamics (DPD) where the solvent is modeled by effective particles interacting with each other and with the lipids via soft potentials. Large-scale DPD simulations of biological membranes have been performed (see, e.g., Refs. 27–29). Multiparticle collision dynamics (MPCD)[30,31] is another method for simulating the dynamics of large systems at mesoscopic level. It is computationally efficient and has been applied with success in a variety of applications.[32,33] In MPCD, real pairwise collisions between solvent molecules are replaced by effective multiparticle collisions between coarse-grain particles which take place inside a lattice of cells. Recently, we have combined the MPCD description for the solvent with a coarse-grain description of lipids to obtain a fast and efficient method for numerical simulations of lipid bilayers.[34] The results of simulations showed that various structural phases of lipid bilayers at different temperatures could be reproduced and experimentally known statistical properties of liquid biomembranes could be recovered.

Interactions between transmembrane[35,36] and peripheral[37,38] inclusions in lipid bilayers have been investigated using DPD. The structures of the inclusions were not resolved and inclusions were modeled as static stiff cylinders spanning or anchored to lipid bilayers. Simulations of passive peripheral proteins interacting with lipid bilayers have been performed using coarse-grain MD and EN models for proteins.[39] Recently, a simple model of an active membrane machine comprising three stiff cylinders with variable links between them was simulated using a coarse-grain description for the lipids and MPCD for the solvent.[40] This model machine can behave as an active swimmer, propelling itself through the membrane.

The aim of the present study is to demonstrate how EN modeling for an active protein machine can be combined with a mesoscopic description for a lipid bilayer, together with the surrounding solvent, to perform fast coarse-grain simulations for active molecular machines in biomembranes. While our approach can be extended straightforwardly to models for real protein inclusions, we study a simple artificial molecular machine whose cycles are based on ligand-induced mechanochemical motions.[17] This model machine mimics the characteristic behavior of actual protein machines (cf. Refs. 41 and 42); its cyclic operation in a solvent has been investigated using MPCD.[22] We consider peripheral protein inclusions, so that our machine does not span the two lipid layers but resides only in one of them. However, the machine is not merely anchored to the membrane: both of its mobile domains have hydrophobic parts and are immersed in the membrane. Under active operation of the machine, the domains move within the membrane and produce hydrodynamic lipid flows. Because the machine has two mobile domains in the membrane, a wealth of interesting behavior can be observed already for a single active inclusion.

In Sec. II, a detailed description of the coarse-grain model of the system is given. The results of simulations of the dynamics of membranes with single active or passive inclusions and their analysis are reported in Sec. III. We show that the membrane is not only statically deformed by passive inclusions, but also dynamically perturbed by the conformational motions of active inclusions. Such conformational motions produce lipid flows which resemble the flows induced by a two-dimensional force dipole. The paper ends with conclusions and a discussion of the results.

II. THE MESOSCOPIC MODEL

The full mesoscopic model comprises coarse-grain models for the lipid bilayer, active protein machine inclusion, and surrounding solvent. The system evolves in time through hybrid MD-MPCD, which combines MD for the protein and lipid molecules in the membrane, and the interactions of these species with the solvent, with MPCD for the solvent.

A. The lipid bilayer membrane

The lipid bilayer model has been given elsewhere[34] and the details of this model will not be repeated here. Briefly, it is based on the model of Cooke *et al.*[24] with potential parameters modified to account for the presence of solvent. Each lipid chain has a hydrophilic head bead (h) and three hydrophobic tail beads (t). Any two lipid beads interact through the truncated repulsive Lennard-Jones potentials. Two neighboring beads inside the same lipid chain are connected by FENE bonds[43] and elastic springs connect next-nearest neighbors in order to account for the bending rigidity of the lipid chain. Hydrophobic effects are taken into account by introducing an additional attractive potential that acts at intermediate distances between tail beads that belong to different lipid chains. Solvent particles and lipid head beads also interact through an attractive potential with shorter attractive range accounting for hydrophilic effects.

B. The molecular machine

Although the molecular machine inclusion is based on a model protein constructed and studied earlier,[17,22] some additional detail is required since the manner in which it interacts with the membrane must be specified. The model machine is represented by an elastic network having $N = 64$ particles connected by elastic springs. The elastic energy of the

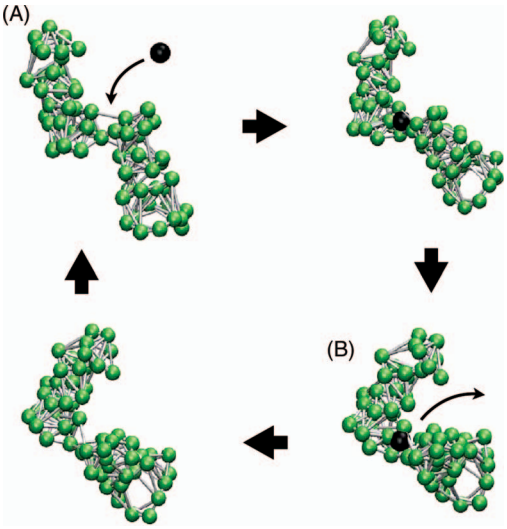

FIG. 1. The cycle of the model machine. Depending on the absence or presence of a ligand (black ball), the machine tends to evolve to the open (A) or closed (B) conformations, respectively.

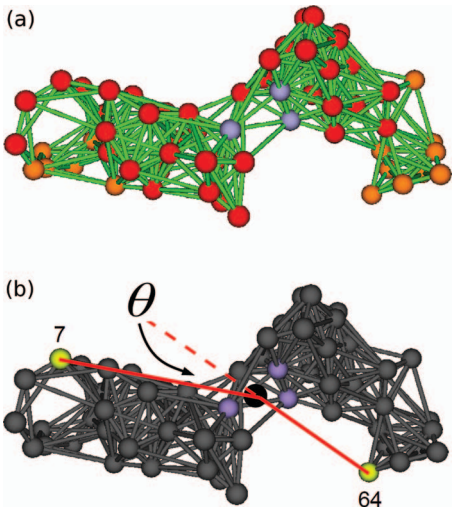

FIG. 2. (a) The molecular machine has 64 beads and 361 interconnecting springs. There are 16 hydrophobic beads (orange), while other beads are hydrophilic (red). Three ligand-binding beads located at the flexible joint are colored purple. (b) The machine conformation is characterized by the hinge angle θ that represents the angle between the vectors connecting two yellow (i = 7 and 64) beads with the center of mass of the binding sites (black).

machine is given by

$$E = \frac{1}{2}k_p \sum_{i=1,j<i}^{N} A_{ij}\left(d_{ij} - d_{ij}^0\right)^2, \tag{1}$$

where k_p is the spring constant, $d_{ij} = |\mathbf{R}_i - \mathbf{R}_j|$ is the distance between particles i and j located at $\mathbf{R}_i$ and $\mathbf{R}_j$, d_{ij}^0 is the equilibrium distance between this pair of particles, and A_{ij} is the matrix of network connections. If two particles i and j are connected by an elastic link, we have $A_{ij} = 1$; otherwise $A_{ij} = 0$. The matrix A_{ij} and the list of equilibrium distances d_{ij}^0 are given in the supplementary online information of Ref. 17. The model machine can be viewed as consisting of two relatively stiff domains (arms) linked by a flexible hinge. It performs cyclic hinge motions powered by ligand binding and unbinding events as illustrated in Fig. 1.

The binding pocket is located in the hinge region and comprises three binding sites ($i = b_1, b_2, b_3$). Binding of the ligand is imitated by placing an additional particle with $i = 65$ at the center of mass of the binding sites and introducing three new elastic links that connect the ligand to the binding sites. The elastic energy E^* of the machine-ligand complex is

$$E^* = E + \frac{1}{2}k_p \sum_{j=1}^{3}\left(d_{65,b_j} - d_{65,b_j}^0\right)^2, \tag{2}$$

where d_{65,b_j} is the distance between the ligand and the particle $i = b_j$ in the binding pocket; d_{65,b_j}^0 is the natural length of the elastic bond that connects two such particles. For simplicity, we assume that the links between the ligand and the three particles in the binding pocket have the same stiffness k_p as in the rest of the network. The natural lengths of additional links are $d_{65,b_1}^0 = d_{65,b_2}^0 = d_{65,b_3}^0 = 0.85\,\sigma$ with $b_1 = 32$, $b_2 = 40$, and $b_3 = 41$. The elastic forces acting on the particle i in the elastic network are given by $\mathbf{F}_i = -\nabla_i E$ or $\mathbf{F}_i = -\nabla_i E^*$ in the presence of the ligand. Here ∇_i is the gradient operator with respect to the position vector $\mathbf{R}_i$ of the ith particle.

The sequence of cyclic conformational transitions shown in Fig. 1 is as follows: When the open conformation of the machine (A) is found near its equilibrium state, binding of the substrate ligand takes place. After binding, a new elastic network representing the machine-ligand complex is formed. This complex undergoes relaxation to its own equilibrium state, corresponding to the closed conformation of the machine (B). When this state is approached, the substrate ligand is transformed into product, which immediately leaves the machine (in terms of the elastic network model, this means that the links connecting the ligand to the machine network suddenly disappear). Subsequently, the free machine relaxes toward its equilibrium open state, where the next ligand may bind so that the cycle is repeated.

To model an active peripheral membrane protein, several particles near the ends of both arms of the machine were made hydrophobic (*pt*),[44] while all other particles in the machine were hydrophilic (*ph*) (see Fig. 2(a)). Interactions between hydrophilic particles of the machine and lipid beads are given by repulsive Lennard-Jones potentials,

$$V_{\alpha\alpha'}(r_{ij}) = 4\epsilon_{\alpha\alpha'}\left[\left(\frac{\sigma}{r_{ij}}\right)^{12} - \left(\frac{\sigma}{r_{ij}}\right)^{6} + \frac{1}{4}\right]\theta(r_c - r_{ij}), \tag{3}$$

where $\alpha, \alpha' \in \{h, t, ph\}$, $\theta(r)$ is the Heaviside function, and $r_{ij} = |\mathbf{r}_i - \mathbf{r}_j|$ is the distance between the beads i and j. The diameter of the beads is determined by the cutoff length $r_c = 2^{1/6}\sigma$, and the interaction strength between beads i and j is $\epsilon_{\alpha\alpha'}$, if bead i is of type α and bead j is of type α'. The hydrophilic particles have different interaction strengths $\epsilon_{ph,h}$ and $\epsilon_{ph,t}$ with the head and tail lipid particles. Hydrophobic particles of the machine interact with lipid head beads through the potential (3) with the cutoff length r_c and the interaction strength $\epsilon_{pt,h}$. Interactions between hydrophobic machine

particles and lipid tail beads are described by an attractive potential,

$$V_{\alpha\alpha'}(r_{ij}) = \begin{cases} 4\epsilon_{\alpha\alpha'}\left[\left(\frac{\sigma}{r_{ij}}\right)^{12} - \left(\frac{\sigma}{r_{ij}}\right)^{6}\right], & r_{ij} < r_c \\ -\epsilon_{\alpha\alpha'}\cos^2\frac{\pi(r_{ij}-r_c)}{2w_{\alpha\alpha'}}, & r_c \le r_{ij} \le r_c + w_{\alpha\alpha'}, \\ 0, & r_{ij} > r_c + w_{\alpha\alpha'} \end{cases} \tag{4}$$

with $w_{\alpha,\alpha'} = w_{pt,t}$ and $\epsilon_{\alpha,\alpha'} = \epsilon_{pt,t}$. Because of hydrophobic interactions between hydrophobic parts of the machine and lipid tails, hydrophobic particles prefer to remain inside the membrane leading to insertion of the machine into the membrane.

Binding and release of the ligand are controlled by the machine conformation. The conformation is characterized by the hinge angle θ shown in Fig. 2(b)). It is defined as the angle between two unit vectors $\hat{r}_1$ and $\hat{r}_2$; i.e., by the equation $\cos\theta = \hat{r}_1 \cdot \hat{r}_2$, where $\hat{r}_1 = (\mathbf{R}_7 - \mathbf{R}_{bs})/|\mathbf{R}_7 - \mathbf{R}_{bs}|$ and $\hat{r}_2 = (\mathbf{R}_{bs} - \mathbf{R}_{64})/|\mathbf{R}_{bs} - \mathbf{R}_{64}|$ with $\mathbf{R}_{bs}$ the position of the center of mass of the three binding sites b_1, b_2, and b_3.

In our simulations, we assume that binding of the ligand is possible inside the interval of the hinge angles defined by the condition $|\cos\theta - \cos\theta_o| < \delta$. Within this interval, binding of ligand occurs with the probability rate ν_o per unit time. Release of the ligand takes place inside the angle window $|\cos\theta - \cos\theta_c| < \delta$ with the probability rate ν_c. We do not allow dissociation of the ligand within the window where its binding may take place. Moreover, we assume that the products are immediately removed, so that the reverse binding of the product after its release and subsequent back reactions are not possible.

C. Interactions with the solvent

Interactions between solvent particles and the hydrophobic and hydrophilic particles of the machine are chosen to be repulsive and are given by Eq. (3) with the same cutoff length r_c, and interaction strengths $\epsilon_{pt,s}$ and $\epsilon_{ph,s}$, respectively. Interactions between solvent particles and lipid beads are the same as in our previous study,[34] where a detailed description can be found. Interactions between solvent particles and lipid tails are purely repulsive with interaction strength ϵ_{ts}, thus taking into account hydrophobic effects. Interactions between solvent particles and lipid heads are repulsive at short range, but attractive at intermediate lengths with the interaction strength ϵ_{hs}; hydrophilic effects are thus included.

D. Hybrid MD-MPC dynamics

The time evolution of the entire system is described by hybrid MD-MPCD, which combines molecular dynamics segments and effective multiparticle solvent collisions at discrete time intervals. Within the molecular dynamics segments, all beads and particles move according to Newton's equations of motion. During this period of time there are no solvent-solvent interactions and the solvent particles only interact with the lipid beads and machine particles through intermolecular potentials. At time intervals τ, multiparticle collisions among solvent particles take place. Such collisions are carried out by sorting solvent particles into the cells of a simple cubic lattice. Particles in the same cell exchange their momentum with each other while the total momentum in the cell is conserved. The constant temperature version of MPCD is employed.[33] For the ith particle in the cell ξ, the collision inside this cell is modeled by updating its velocity, $\mathbf{v}_i$, so that the new velocity, $\mathbf{v}_i'$ is given by

$$\mathbf{v}_i' = \mathbf{V}_\xi + \mathbf{v}_i^{ran} - \sum_{j\in\text{cell }\xi} \mathbf{v}_j^{ran}/N_\xi, \tag{5}$$

where $\mathbf{V}_\xi$ is the mean velocity of the particles in the cell ξ, and the components of $\mathbf{v}_i^{ran}$ are chosen to be Gaussian random numbers with zero mean and variance k_BT/m. The summation is performed over N_ξ solvent particles inside the cell ξ. Since the mean free path of the solvent particles in our simulations was small compared with the size of a MPC cell, we have used random grid-shifting[45,46] to implement the MPC step. Additional details and applications of MPCD can be found in review articles.[32,33]

E. Parameter values

In this section we give numerical values of all parameters used in our simulations and specify the initial and boundary conditions that were employed. Some of the parameters were introduced in our previous publication dealing with the lipid bilayer,[34] which should be consulted for further information. The characteristic interaction energies between different types of beads were $\epsilon_{ht} = 1\,\epsilon$, $\epsilon_{hs} = \epsilon_{ph,s} = 0.05\,\epsilon$, $\epsilon_{ts} = \epsilon_{pt,s} = 2.0\,\epsilon$, $\epsilon_{hh} = \epsilon_{tt} = \epsilon_{pt,t} = 0.5\,\epsilon$, and $\epsilon_{ph,h} = \epsilon_{ph,t} = \epsilon_{pt,h} = 5.0\,\epsilon$. The attraction ranges for tail-tail and solvent-head interactions were chosen such that $r_c + w_{tt} = 2.6\,\sigma$ and $r_c + w_{sh} = 1.65\,\sigma$. The attractive range for a machine hydrophobic particle and a lipid tail bead was $w_{pt,t} = w_{tt}$. Lipid beads and solvent particles had equal masses $m_\ell = m_s = m$, while the mass of the machine particles was $m_p = 10\,m$. The simulations were carried out in a rectangular box of size $40\,\sigma \times 40\,\sigma \times 25\,\sigma$ with periodic boundary conditions. The lateral size of a MPC cell was $a_0 = \sigma$. The system contained one model machine, 2560 lipid chains, and 140 784 solvent particles.

The machine dynamics in a solvent was investigated earlier using MPCD.[22] In the present study, we chose a higher temperature to ensure that the membrane was in the liquid phase characteristic of that for real biological membranes. Since thermal noise was stronger at higher temperatures, the machine was made stiffer than in Ref. 22, with a larger spring constant $k_p = 6000\,\epsilon/\sigma^2$. In addition, the natural lengths of all springs were shortened by a factor of two, thus making the machine smaller. The machine was in the open state when $\cos\theta \approx \cos\theta_o = 0.71$ and in the closed state when $\cos\theta \approx \cos\theta_c = 0.11$. The ligand binding and release conditions were determined by the parameter $\delta = 0.05$; the binding and release rate constants were chosen as $\nu_o = \nu_c = 0.1$.

The initial velocities of all particles were Gaussian distributed with zero mean and variance k_BT/m_α for each component, where $\alpha = \ell, s$, and p. For the MD trajectory segments, Newton's equations of motion were integrated using

the velocity-Verlet algorithm with a time step of $\delta t = 0.005\, t_0$, where $t_0 = \sqrt{m\sigma^2/\epsilon}$. The MPC time step was $\tau = 0.2\, t_0 = 40\, \delta t$. At the beginning of the simulations, the model machine was prepared in the closed conformation, and the hydrophobic beads were immersed in the membrane. The simulation data were collected after the system evolved for $10^5\, \delta t$, so that a new steady state was established. The numerical results are reported below in dimensionless units. We have chosen σ to be the unit of length and m the unit mass. The characteristic interaction energy between a lipid head and a lipid tail bead, $\epsilon_{ht} \equiv \epsilon = k_B T$, was taken to be the unit energy. Time is reported in units of δt.

With the parameters for lipid-lipid and lipid-solvent interactions described above, self-assembly of a membrane from an initially uniform mixture of lipids was observed, and the resulting membranes were in liquid phase.[34]

III. SIMULATION RESULTS

Simulations of the dynamics of the active and passive (ligand-free or ligand-bound (Fig. 3)) molecular machines in a lipid bilayer have been carried out and videos for both cases are available in the online information.

The results of these simulations show that the membrane-associated machines remain attached to the membrane; however, both of their arms are located only within one lipid leaflet, a situation that characterizes peripheral proteins.

Interactions with the membrane affect the machine dynamics. More specifically, the hinge angle of the membrane machine in its ligand-free open conformation is larger (with the maximum at about $\cos\theta_{max} \simeq 0.85$) than that for the same machine in the absence of a membrane ($\cos\theta \simeq 1.0$). The lipids close to the ends of the opening arms are pulled up and the lipids close to the center of the machine are pushed downward by the machine. The forces generated by the deformed membrane and applied to the machine arms do not allow the machine to completely open and thus increase the hinge angle. By contrast, the ligand-bound closed conformation of the membrane machine is not strongly affected by the interactions with lipids, and its hinge angle is about the same as that for the machine in a solvent ($\cos\theta \simeq 0.17$). Thus, the machine perturbs the membrane more strongly if it is in the ligand-free open conformation.

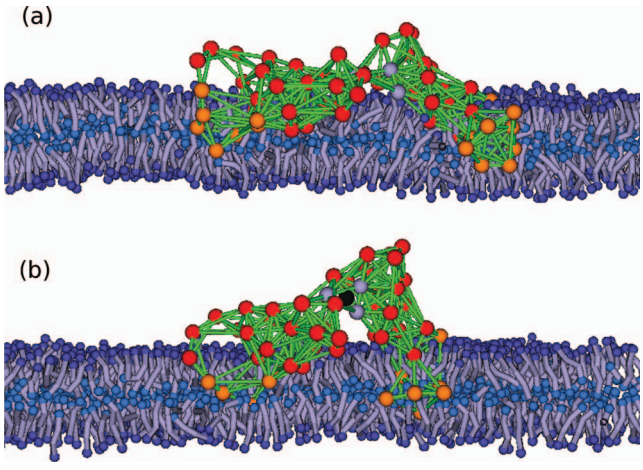

FIG. 3. Membranes with the immersed ligand-free (a) and ligand-bound (b) machines. Each lipid is represented by a flexible rod. The blue beads are the hydrophilic head beads, the light blue beads are the last tail beads of the lipid chains, the gray rods represent the hydrophobic part of the lipid chains, and the ligand is shown as a black bead. The solvent is not displayed, and only half of membrane is shown for clear visualization (enhanced online). [URL: http://dx.doi.org/10.1063/1.4803507.1] [URL: http://dx.doi.org/10.1063/1.4803507.2]

A. Effects of passive inclusions

Lipid bilayer membranes are deformable objects, and the deformations in the thickness and the height of the membrane are analyzed below. We begin our statistical analysis by considering membrane deformations induced by passive inclusions, i.e., by machines where binding or detachment of the ligands is suppressed so that active cycling is absent. Generally, the presence of an inclusion can lead to local compression and to local bending of the membrane. The local thickness of the membrane can be used to monitor local compression while the local membrane height can be used as a probe for the local bending of the membrane; both properties are considered for passive inclusions representing ligand-free and ligand-bound machines.

To quantitatively describe membrane deformations, averages over 2000 system configurations separated by $500\, \delta t$ were performed for both cases. For each configuration, the system was shifted and rotated so that the center of mass of the machine was always located in the center of the membrane and the machine was always orientated along the diagonal line in the xy-plane. Through such *a posteriori* adjustment, we could compare the induced membrane deformation profiles irrespective of the actual position and orientation of the machine.

In each system configuration, the lipid beads were sorted according to their positions into a grid of 16×16 cells in the xy-plane with linear cell size $2.5\, \sigma$. In the cell (x, y), the midplane height, $h_m(x, y)$, was measured by averaging the z-components of the positions of all the terminal lipid-tail beads in this cell, and the membrane thickness was defined as $h_d(x, y) = h_u(x, y) - h_l(x, y)$, where $h_u(x, y)$ and $h_l(x, y)$ are the heights of the upper and the lower leaflets, respectively. The heights of the leaflets were determined by averaging the z-components of the positions of the lipid head beads. A lipid was taken as being in the upper or lower leaflets by identifying the z-component of its head bead ($r_{h,z}$) and its terminal tail bead ($r_{t,z}$). If $r_{h,z} > r_{t,z}$, this lipid was in the upper leaflet, and in the lower leaflet otherwise.

Note that our definition of midplane height is different from the conventional definition,[1,47] where the average height of the upper and the lower leaflets were taken. Together with the membrane thickness, the elastic deformations of a membrane were described by these two fields.[1,47] Since our molecular machine is attached to only one membrane leaflet, the membrane leaflets are expected to be differently deformed. Therefore, in this work we use three fields h_u, h_l, and h_m to describe membrane shape.

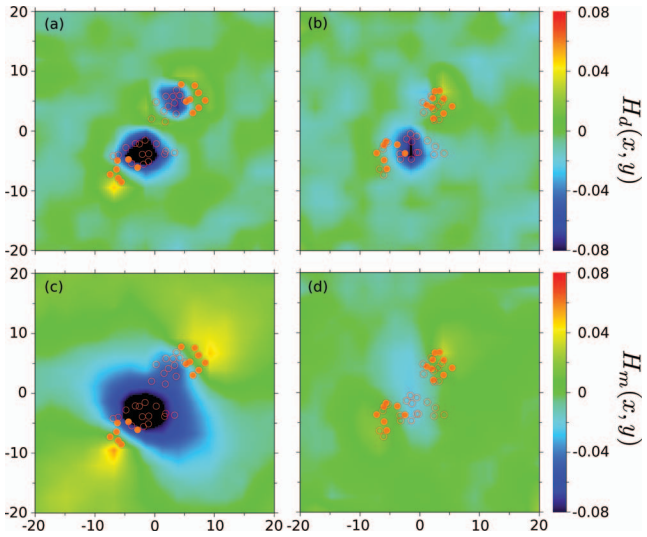

FIG. 4. Thickness (upper row) and midplane height (lower row) of the membrane with the ligand-free (left column) and ligand-bound (right column) machines immersed in the upper membrane leaflet. Normalized values of the membrane thickness and midplane height are displayed by using the color codes shown in the bars. Filled orange circles mark average positions of the hydrophobic beads of the machine, whereas open circles correspond to the machine hydrophilic beads which are immersed in or are in contact with the membrane.

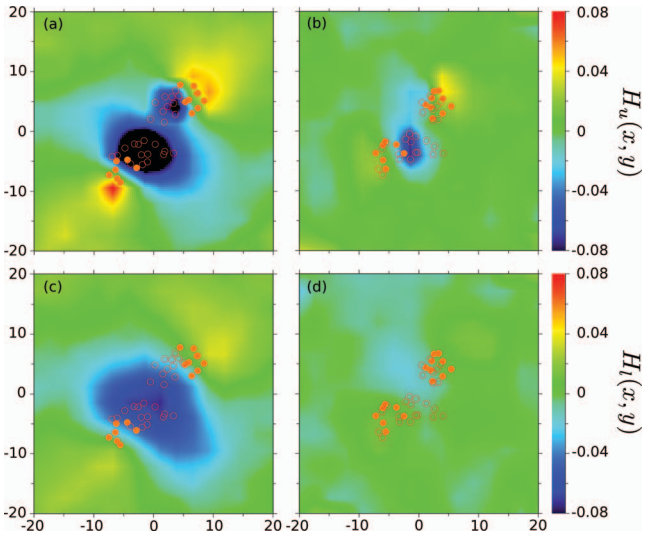

FIG. 5. Heights of the upper (upper row) and the lower (lower row) leaflets with ligand-free (left column) and ligand-bound (right column) machines. Normalized heights are displayed by using the color codes shown in the bars. Solid orange circles mark average positions of the hydrophobic beads of the machine, whereas open circles correspond to the machine hydrophilic beads which are immersed into or are in contact with the membrane.

Figures 4(a) and 4(b) show the normalized thickness $H_d(x, y) = \langle h_d(x, y) - d_0\rangle/d_0$ for the membranes with passive ligand-free and ligand-bound machines, respectively. Here $\langle\cdots\rangle$ denotes an average over all system configurations and $d_0 \sim 5.5\,\sigma$ is the mean thickness of the machine-free membrane.[34] In addition, we have displayed the average positions of hydrophobic particles (solid orange circles) and hydrophilic particles (open circles) which are immersed in the membrane or are in contact with it. Note that the upper-right and the lower-left hydrophobic particles in these figures correspond to the right and the left arms of the machine shown in Fig. 3. As expected from Fig. 3(a) for the ligand-free machine, the lipids that are close to the hydrophobic machine particles were found to strongly interact with the hydrophilic particles of the machine, resulting in two thinned domains with the lateral sizes between $5\,\sigma$ and $10\,\sigma$ (see Fig. 4(a)), comparable to the size of the hydrophobic part of the machine projected onto the membrane. For the ligand-bound machine in Fig. 4(b), only one thinned domain at the left arm is seen.

The normalized midplane heights of the membrane, $H_m(x, y) = \langle h_m(x, y) - h_m^0\rangle/d_0$, with ligand-free and ligand-bound machines are shown in Figs. 4(c) and 4(d); here h_m^0 is the instantaneous mean midplane height. In contrast to the compression, which is localized in narrow regions corresponding to the immersed parts of the arms, membrane bending extends over a lager area comparable with the size of the entire machine. Furthermore, while substantial bending is induced by the ligand-free machine, only weak membrane bending is found if a passive machine with a ligand is present. These findings indicate that membranes are compressed and bent in the presence of forces exerted by the molecular machine.

In contrast to previous studies[35,36] where passive transmembrane inclusions spanning both membrane monolayers were considered, our machine inclusions correspond to peripheral proteins and are immersed in only one membrane monolayer (leaflet). Therefore, depending on which leaflet is considered, deformation effects may be different. Below, we investigate such differences by determining the heights of two membrane leaflets.

The average heights of the upper and lower leaflets with both types of passive machines were obtained by using the *a posteriori* adjustment procedure described above. In the cell (x, y), we calculated the normalized average local heights $H_u(x, y) = \langle h_u(x, y) - h_u^0\rangle/d_0$ and $H_l(x, y) = \langle h_l(x, y) - h_l^0\rangle/d_0$ of the upper and the lower leaflets, where h_u^0 and h_l^0 were the instantaneous mean heights of these leaflets.

Figures 5(a) and 5(c) show $H_u(x, y)$ and $H_l(x, y)$ for the membrane with a passive ligand-free machine. As might be expected, in the upper leaflet the lipids were pressed down by the hydrophilic particles so that two depressions were formed, and the lipids near the ends of the hydrophobic parts were raised by the opening arms so that two elevations were found there (Fig. 5(a)). Such deformations extended over an area comparable with the size of the inclusion. Similar deformations were found in the lower leaflet (see Fig. 5(c)), but their magnitudes were significantly smaller.

For the membranes with passive ligand-bound machines, noticeable changes were found only in the upper leaflet near the ends of machine arms (Fig. 5(b)), and the effects on the lower leaflet were negligible (Fig. 5(d)).

B. Effects of active inclusions

Our active membrane machine cyclically changes its conformation, alternating between the open and closed states, as

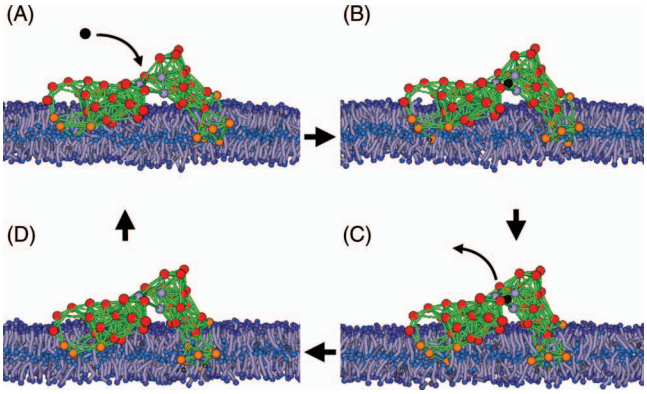

FIG. 6. The cycle of a membrane machine: (A) The ligand binds to the machine; (B) the machine conformation changes from the open state to the closed state; (C) the reaction takes place and the ligand is released; (D) the machine returns to its open state (enhanced online). [URL: http://dx.doi.org/10.1063/1.4803507.3]

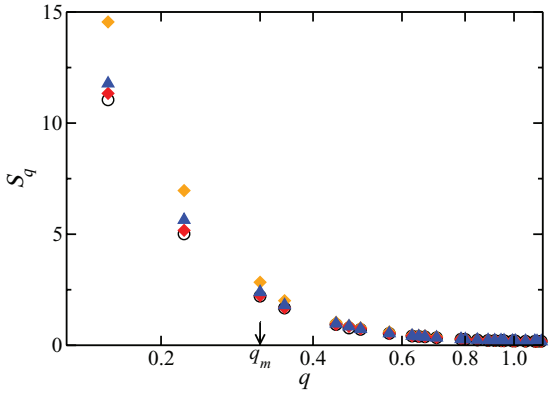

FIG. 8. The power spectrum of the free membrane (black circles), of the membrane anchored with a passive closed machine (red solid diamonds), the membrane anchored with a passive open machine (yellow solid diamonds), and the membrane anchored with an active machine (blue solid triangles).

illustrated in Fig. 6. (The video for the active membrane machine is available in the online information.) When the substrate ligand arrives (A), the machine swings its arms downward (B→C) and presses the membrane until the machine reaches the closed state where the ligand is in a favorable environment for conversion to product, which is then released. After the ligand has left the machine (C), the membrane is locally pulled upward by the opening arms (D→A). In our simulations, such cyclic conformational motions are traced by monitoring the machine hinge angle. The evolution of the hinge angle over 7 typical cycles is shown in Fig. 7. Thus, repeated membrane deformations, comprising its local bending and thinning, take place when the machine is active. Moreover, since the immersed arms of the machine actively move apart or towards one another through the membrane, hydrodynamical flows within lipid leaflets can be induced. Both of these effects have been considered in our simulations and their statistical analysis.

First, we consider how an active machine influences the shape of the membrane. In contrast to the study of passive machines, information contained in the average membrane profiles is no longer sufficient for this purpose, and instead shape

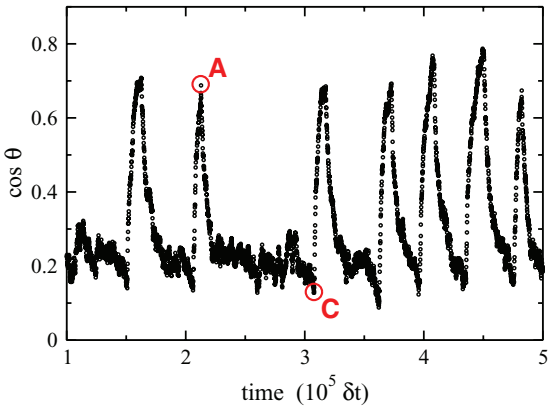

FIG. 7. Hinge angle of an active machine as a function of time. The label A marks a ligand-binding event, while C marks a ligand-releasing event as shown in Fig. 6.

fluctuations of the membrane were analyzed. To determine the power spectrum of height fluctuations, membrane configurations were recorded every 10000 δt and, in total, 1000 membrane configurations were collected for analysis. In each configuration, the membrane was divided into 16×16 cells, and the midplane height of each cell was measured by the mean positions of the last tail beads. Then, the power spectrum of each membrane configuration was obtained by performing a fast Fourier transform of the midplane heights. By averaging over all membrane configurations, the average power spectrum was obtained.

Figure 8 shows the power spectrum of height fluctuations of the membrane $S_q = L_0^2 \langle |h_m(\mathbf{q})|^2 \rangle$ with an active machine (blue solid triangles). For comparison, we have also measured the power spectrum of the same membrane without a machine (black circles) and of the membrane with passive machines in the presence or absence of ligands (red solid diamonds and yellow solid diamonds). From an examination of this figure, we see that the presence of inclusions affects the power spectrum of height fluctuations and the effect depends on the conformational state and the activity of these inclusions. However, significant changes are found only for sufficiently small wavenumbers $q < q_m$, where q_m is approximately 0.3. This characteristic wavenumber corresponds to the length of about $L_m = 20\,\sigma$ which is close to the linear size of the membrane machine. We can also see that the strongest influence on the height fluctuations spectrum is for a machine in the ligand-free open conformation. This is consistent with our previous observations (Figs. 4 and 5) since, in this conformation, the machine most strongly perturbs the local height and the thickness of the membrane. Note that the analysis of S_q based on the experimental data for the transmembrane bacteriorhodopsin protein has previously shown that the surface tension of the membrane with the active form of the protein was significantly lower than that with the passive form.[5] In our simulations, we found that the surface tensions of the membranes with a ligand-free machine and a ligand-bound machine were $\sim 3.05\,\epsilon/\sigma^2$ and $3.10\,\epsilon/\sigma^2$, respectively, and the surface tension was $\sim 3.09\,\epsilon/\sigma^2$ for the membranes with an active machine. Therefore, in going from passive to active

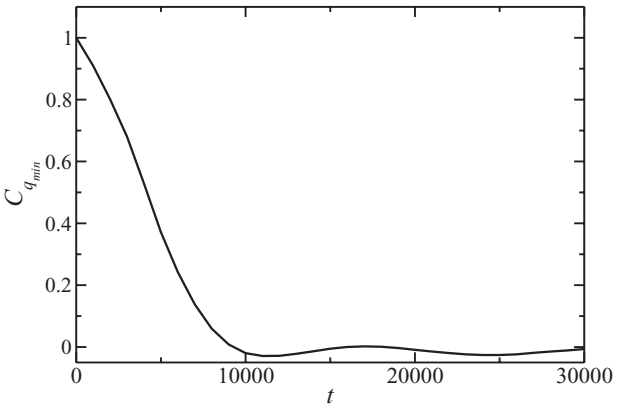

FIG. 9. Time autocorrelation function of the height fluctuation $C_{q_{min}}$ for the membrane without a machine.

peripheral proteins, only a small change in the surface tension is observed in the model which we consider.

From Fig. 8, we see that fluctuations of a membrane with an active machine are smaller than those of a membrane with a passive ligand-free machine and are only slightly stronger than that for a passive ligand-bound machine. By examining the time series of the hinge angle (see Fig. 7), it can be noticed that, within a machine cycle, the machine spends much time in the closed conformation waiting for the ligand to be released. This explains why the fluctuations of a membrane with an active machine are closer to those of a membrane with a passive machine in the closed conformation.

To analyze height fluctuations further, the autocorrelation function $C_{q_{min}}(t) = \langle h_{q_{min}}(t) h_{-q_{min}}(0) \rangle$, where $h_{q_{min}}$ is the Fourier component of the membrane height with smallest wave number $q_{min} = 2\pi/L_0$, was determined (Fig. 9). Here L_0 is the linear size of the membrane. As we see from this figure, the correlation time of such fluctuations is about $\tau_c = 5000\,\delta t$. We also determined the average time for the machine opening and closing processes, where the opening process started from ligand release and finished when the hinge angle first entered the ligand binding window and the closing process started from ligand binding and finished when the hinge angle first entered the ligand release window. Examining data in Fig. 7, we find that the mean closing time is about $25\,000\,\delta t$; hence, conformation changes after ligand binding are significantly slower than the characteristic timescales of membrane shape fluctuations in our simulations.[48] On the other hand, the average time for the opening processes is about $8000\,\delta t$, comparable to the membrane relaxation time. Therefore, the fluctuations of the membrane at this length scale could adiabatically follow the slow closing processes, but may be on the same timescale with the fast opening motions of active machines. If the membrane size L_0 is increased, height fluctuations with smaller wavenumbers q_{min} can be obtained and the relaxation of such fluctuations would be slower. There may be a stronger interplay between such slow membrane fluctuations and machine cycles. However, simulations with significantly larger membrane systems could not yet be undertaken in the present study.

C. Lipid flows induced by an active machine

From an examination of velocity correlation functions of lipid flows, we showed previously[34] that a lipid bilayer can be treated as a two-dimensional fluid with a logarithmic distance dependence characteristic for hydrodynamic interactions in two dimensions.[49] When an active membrane machine is present, its conformational motions not only affect the membrane shape but also laterally stir the lipid bilayer so that lipid flows can be expected.

To compute the velocity field of such lipid flows, ten independent simulations were carried out. In each simulation a system configuration was recorded every $10\,\delta t$ giving, in total, 100 000 configurations for analysis. For each configuration, the mean velocity and the mean position of each lipid molecule, determined from averages of the velocities and positions of its beads, were computed. Again, the positions of all lipid and machine beads were shifted and rotated so that the machine was brought to the membrane center and oriented along the diagonal line in the xy-plane. When rotating the system, the lipid velocities were also rotated using the same rotation operation as for the lipids. The lipids were then sorted into a grid of 16×16 cells, and the average velocity in each cell was averaged over the lipids within the cell. To reduce the dispersion of the data, additional time averaging was carried out. Such averaging should be carried out on configurations with similar machine conformations. An examination of machine motions showed that machine arms immersed in the membrane move fastest immediately after binding or release of a ligand. Hence, the strongest effects on the lipid flows are to be expected at such cycle stages. Having this in mind, we identified the initial opening and closing segments in each cycle. The closing segment starts from ligand binding and ends at the moment when $\cos\theta$ first becomes greater than $\cos\theta_t$, whereas the opening segment starts from ligand detachment and ends at the moment when $\cos\theta$ first becomes smaller than $\cos\theta_t$. The characteristic angle θ_t was chosen as $\theta_t = (\theta_o + \theta_c)/2$, i.e., the average of the hinge angles for the open and closed conformations. The configurations corresponding to the opening and closing segments in each machine cycle were selected and separate averaging over all such configurations for a series of five simulations was performed. As a result, average lipid fields corresponding to the opening and closing stages of an active machine could be determined.

The pronounced flows in the lipid bilayer, induced by the opening and closing motions of the membrane machine, can be seen in Fig. 10, where the colors specify the magnitude of the velocity and the arrows indicate the local direction of the lipid flow. The lipids stream together with the opening arms in the upper-right and the lower-left directions. At the same time, the lipids from the periphery flow into the space between the two arms along the transverse directions. The velocity field for the closing segment is shown in Fig. 10(b). As expected, the direction of the flow field is roughly reversed. The magnitudes of the lipid velocity fields also correlate with the speeds of the machine arms. For the opening segments, the hydrophobic domains of the lower-left arm (arm 1) and the upper-right arm (arm 2) were found to move with average speeds $v_1^o \simeq 0.11$ and $v_2^o \simeq 0.12$, respectively; for the

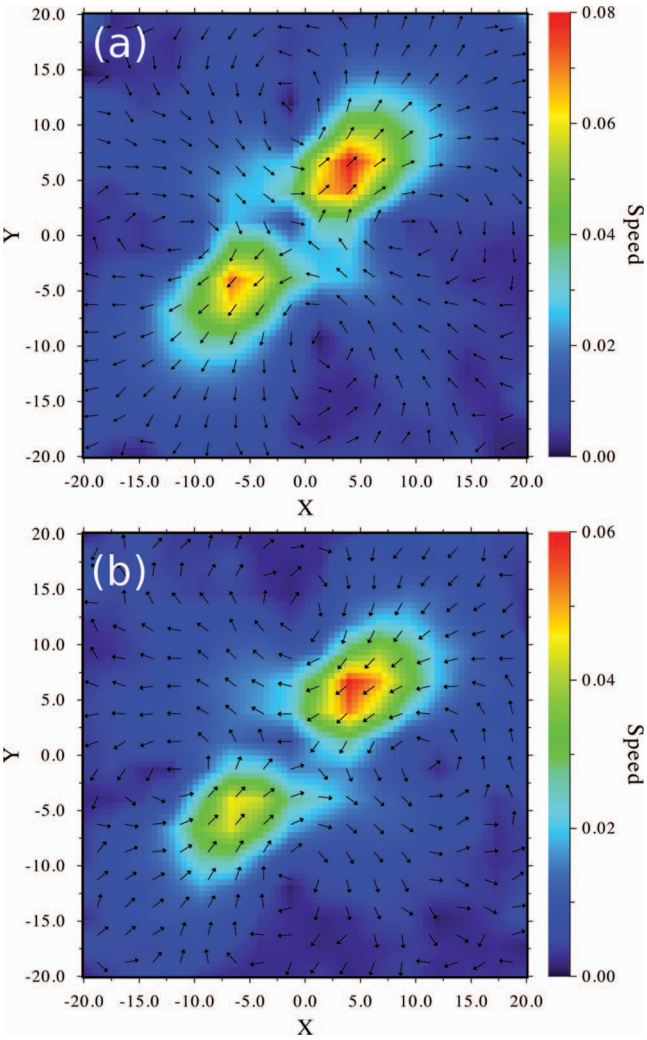

FIG. 10. Average lipid velocity fields for (a) opening segments and (b) closing segments. The arrows indicate the direction of the velocity and the colors characterize the flow speed.

closing segments, the average speeds of these domains were $v_1^c \simeq 0.07$ and $v_2^c \simeq 0.08$. These magnitudes are comparable to the maximum lipid flow speeds for the opening and closing segments, ~0.08 and 0.06, respectively.

Comparing the distributions for the membrane deformations (Figs. 4 and 5) and the lipid velocity fields (Fig. 10), we notice that, in contrast to the membrane thickness changes, the induced lipid flows are not localized in the immediate vicinity of the immersed machine domains. This is related to the fact that the membrane behaves as a two-dimensional fluid on the length scale which we consider. According to the existing theories[49,50] and confirmed in our earlier simulations,[34,40] lipid bilayers represent two-dimensional Navier-Stokes fluids on the scales shorter than a micrometer. On such scales, lipid flows in the membrane are decoupled from the flows in the solvent, so that hydrodynamical slip conditions apply.

In addition, we employed an immobilization procedure by applying compensating forces on the machine particles (see Appendix A), and measured the average forces acting on the rigid arms in the initial opening and closing segments: $\langle F'^{o,c}_{\kappa,\beta}\rangle = \langle \sum_{i\in\kappa} f'^{o,c}_{i,\beta}\rangle$, where $\beta = x, y$, $\kappa = 1, 2$ denotes arms 1 and 2, respectively, $f'_{i,\beta}$ is the net force on particle i in arm κ, including intermolecular forces and compensating forces, and $\langle\cdots\rangle$ denotes the average over approximately 300 opening and closing segments. We have $\mathbf{F}'^{o,c}_1 = -\mathbf{F}'^{o,c}_2$ since the machine is immobilized; we found that $|F'^{o}_1| = |F'^{o}_2| \simeq 0.64$ and $|F'^{c}_1| = |F'^{c}_2| \simeq 0.40$. Since our machines operate in a low Reynolds number environment,[22,40] the velocities of the arms are proportional to the forces. The ratio $|F'^{o}|/|F'^{c}| \simeq 1.6$ is comparable to both the ratio of the maximum lipid flow speeds driven by the opening-closing segments of the machine cycles (see Fig. 10), and the ratio of the arm speeds.

The hydrodynamical lipid membrane flow effects arising from the conformational motions of a membrane machine are similar to those seen for an organism swimming in a fluid medium. For example, recent experiments[51] on the flow fields induced by the nonreciprocal swimming motions of the single-celled alga *Chlamydomonas reinhardtii* in a quasi two-dimensional medium lead to flow patterns like those of our much smaller molecular machine. In particular, as can be seen in panels (a) and (f) of Fig. 3 of this reference, the flow fields for the power and recovery strokes of this microorganism have the same structure as those produced by the opening and closing motions of our molecular machine. These induced flow patterns resemble the fluid velocity fields of hydrodynamical negative and positive force dipoles.[51]

A more detailed assessment of the force dipoles can be obtained from the force dipole moment for the opening and closing segments. The immobilization procedure was again employed so that there was no net force and torque on the machine (Appendix A). The force dipole moment in two dimensions is a second rank tensor $\tilde{\mathbf{P}}$,[52] and the average of the elements of the tensor was determined by

$$\langle \tilde{P}_{\beta\beta'}\rangle = \left\langle \sum_{\kappa=1}^{2} R_{cm,\kappa\beta} F'_{\kappa\beta'} \right\rangle, \tag{6}$$

where $\beta, \beta' = \{x, y\}$ and $R_{cm,\kappa\beta}$ is the position of the center of mass of the machine arm κ. Note that only the contributions from large conformational motions of the machine arms were considered in Eq. (6) (see details in Appendix B). From the average over approximately 300 opening and closing events, we found the eigenvalues of $\langle\tilde{\mathbf{P}}\rangle$ for the opening processes were $\lambda^o \simeq 1.66$ and -0.72, and those for the closing processes were $\lambda^c \simeq -6.74$ and -0.79. For the opening segment, the positive eigenvalue corresponds to the extension of the arms along the machine orientation indicating a force dilatation dipole, and the small negative eigenvalue represents the small contraction in the perpendicular direction. While a small negative eigenvalue was also determined in the closing segment, there exists negative eigenvalue with larger magnitude, which indicates a force contraction dipole.

Because membrane-bound machines are very small, with dimensions on nanometer scales, they are subject to strong thermal fluctuations. Consequently, as noted above, full details of the lipid flow fields induced by our molecular machine are only revealed after extensive averaging.

IV. DISCUSSION AND CONCLUSIONS

Understanding the dynamical properties of membrane bound protein machines is an important task because of the prevalence of such proteins and the roles they play in biological function. The mesoscopic method described in this paper provides a way to study their behavior through molecular simulation. Several features of the mesoscopic model are worth reviewing: the lipid membrane, protein machine, and solvent are all modeled at coarse-grain particle level. This allows large-scale simulations to be carried out efficiently. While the model is mesoscopic in character, since momentum is conserved, hydrodynamic interactions that are responsible for fluid flows induced in the membrane by machine motions are taken into account. The extension of the elastic network description to realistic models of specific protein machines[18–20,23,53] is straightforward and has the potential to allow one to explore aspects of the dynamical functions of membrane bound proteins that occur in the cell.

A number of other features of the mesoscopic model make it an attractive method for the study of membrane-bound protein machines and proteins in general. Since interactions between the particles forming the protein inclusion, lipids, and the solvent are treated through specific intermolecular potentials, both hydrophilic and hydrophobic interactions can be taken into account. In our study, both passive and active proteins were investigated. A passive machine deforms the lipid bilayer structure giving rise to distinctive local changes in thickness and bending of the membrane leaflets. Active machine cycling also gives rise to long ranged hydrodynamic flows in the membrane. Since intrinsic thermal fluctuations are strong for these nanoscale machines, substantial averaging is needed in order to observe and analyze the systematic flows induced by machine domain motions. The ability of the mesoscopic simulation method to address all of these factors makes it a powerful tool for the study of active membrane-bound protein machines.

The existence of induced lipid flows gives rise to long-range interactions between membrane proteins, which may play an important role in their collective dynamics. It should be noted that such flows, and the long-range hydrodynamical interactions they produce, will only be present if the protein inclusions are active, i.e., they cyclically change their conformation. Investigations of interactions between active protein machines in biomembranes is the subject of future research.

ACKNOWLEDGMENTS

Financial support from the DFG Research Training Research Group (GRK 1558) "Nonequilibrium Collective Dynamics in Condensed Matter and Biological Systems" (Germany) is gratefully acknowledged. Research of R.K. was supported in part by a grant from the Natural Sciences and Engineering Research Council of Canada, and through the Research Award of the Humboldt Foundation in Germany. The research of M.J.H. and H.Y.C. is supported by the National Science Council of Taiwan (NSCT) under Grant No. NSC 101-2112-M-008-002 and by the National Center for Theoretical Sciences, Taiwan. Some computations were performed on the GPC supercomputer at the SciNet HPC Consortium.[54] SciNet is funded by: the Canada Foundation for Innovation under the auspices of Compute Canada; the Government of Ontario; Ontario Research Fund-Research Excellence; and the University of Toronto.

APPENDIX A: IMMOBILIZATION PROCEDURE

When an active peripheral machine cyclically changes its conformation in a membrane, the interactions with surrounding solvent and lipid molecules may induce translational motions in the x and y (lateral) directions and rotational motions about z (membrane normal) direction. In order to compensate the forces that induce such motions without affecting the machine conformational dynamics, we have employed an immobilization procedure.

A machine particle i experiences a net force $\mathbf{f}_i$ comprising intermolecular forces and spring forces in the elastic network, and the total force acting the machine is

$$\mathbf{F} = \sum_{i=1}^{N} \mathbf{f}_i, \tag{A1}$$

where $N = 64$ is the number of particles in the machine. To immobilize the translational motions of the machine, a compensating force $\mathbf{f}_t = -\mathbf{F}/N$ is applied to all particles in the machine. In addition, the net forces acting the machine particles also generate a torque,

$$\mathbf{T} = \sum_{i=1}^{N} (\mathbf{R}_i - \mathbf{R}_{cm}) \times \mathbf{f}_i, \tag{A2}$$

where $\mathbf{R}_i$ is the position of particle i and $\mathbf{R}_{cm}$ is the position of the center of mass (CM) of the machine. To compensate the torque, an external force $\mathbf{f}_{r,i} = \boldsymbol{\omega} \times \mathbf{R}_i$ is added to particle i. Here $\boldsymbol{\omega}$ is an arbitrary vector which should be chosen such that

$$\mathbf{T} + \sum_{i=1}^{N} (\mathbf{R}_i - \mathbf{R}_{cm}) \times \mathbf{f}_{r,i} = 0. \tag{A3}$$

Note that in our simulations, only the rotational motion about the membrane normal (z-direction) is prevented. To do this, we find that

$$\omega_z = \frac{-T_z}{\sum_{i=1}^{N} |\mathbf{R}_i - \mathbf{R}_{cm}|^2}, \tag{A4}$$

and thus the external force on particle i is

$$\mathbf{f}_{r,i} = \frac{-T_z \hat{\mathbf{z}} \times (\mathbf{R}_i - \mathbf{R}_{cm})}{\sum_{i=1}^{N} |\mathbf{R}_i - \mathbf{R}_{cm}|^2}. \tag{A5}$$

The initial velocity of the machine particles is chosen so that the linear and angular momenta vanish. At each MD step, the compensating forces are included in the equations of motion, and the force acting on particle i becomes

$$\mathbf{f}_i' = \mathbf{f}_i + \mathbf{f}_t + \mathbf{f}_{r,i}. \tag{A6}$$

One may verified that $\sum_i \mathbf{f}_i' = 0$ and $\sum_i (\mathbf{R}_i - \mathbf{R}_{cm}) \times \mathbf{f}_i' = 0$, thus the CM translational and z-rotational motions are eliminated.

APPENDIX B: FORCE DIPOLE MOMENT

In our simulations, while the model peripheral machine operates in a three-dimensional space, the induced flow pattern shown in Fig. 10 suggests that the machine behaves like a two-dimensional force dipole during its opening and closing processes.

In general, consider a protein machine consisting of n domains. The force dipole moment, a second rank tensor, is defined as

$$P_{\beta\beta'} = \sum_{\kappa=1}^{n} \sum_{i\in\kappa} R_{i\beta} f'_{i\beta'}, \tag{B1}$$

where $\beta, \beta' = \{x, y\}$, $R_{i\beta}$ is the β-component of position of the particle i, and $f'_{i\beta'}$ is the β'-component of the force given in Eq. (A6). We notice that the position of particle i in domain κ can be written as $\mathbf{R}_i = \mathbf{R}_{cm,\kappa} + \delta\mathbf{R}_i$, where $\delta\mathbf{R}_i$ is the deviation from the CM of domain κ, and Eq. (B1) becomes

$$P_{\beta\beta'} = \sum_{\kappa=1}^{n} R_{cm,\kappa\beta} F'_{\kappa\beta'} + \sum_{\kappa=1}^{n} \sum_{i\in\kappa} \delta R_{i\beta} f'_{i\beta'}, \tag{B2}$$

where $F'_{\kappa\beta'} = \sum_{i\in\kappa} f'_{i\beta'}$ is the total force acting on domain κ. In our model machine, there are two rigid domains (n = 2). The first term in the right side of Eq. (B2) corresponds to the contributions from the large conformational motions of two rigid arms inducing lipid flows, and the second term is the contribution to the force dipole from forces that lead to motions relative to the CM of the machine arms.

In our studies, we focus on the effects due to conformational motions of the machine arms, therefore only $\tilde{P}_{\beta\beta'} = \sum_{\kappa=1}^{n} R_{cm,\kappa\beta} F'_{\kappa\beta'}$ is considered. Generally, $\tilde{\mathbf{P}}$ is not a diagonal matrix since the machines in our simulations could be orientated in an arbitrary direction in the xy-plane. Diagonalization of $\tilde{\mathbf{P}}$ yields two eigenvalues λ_1 and λ_2 with corresponding eigenvectors Λ_1 and Λ_2. If $\lambda_i > 0$, the machine conformational motion corresponds to a force dilatation dipole in the direction along the eigenvector Λ_i, and for a force contraction dipole the eigenvalue λ_i is negative.[52]

[1] R. Phillips, J. Kondev, and J. Theriot, *Physical Biology of the Cell* (Garland Science, 2009).
[2] A. Arkhipov, Y. Yin, and K. Schulten, Biophys. J. **95**, 2806 (2008).
[3] A. Callan-Jones and P. Bassereau, Dev. Cell **22**, 691 (2012).
[4] H. Lodish, A. Berk, C. A. Kaiser, M. Krieger, M. P. Scott, A. Bretscher, H. Ploegh, and P. Matsudaira, *Molecular Cell Biology*, 6th ed. (W. H. Freeman, 2007).
[5] M. D. El Alaoui Faris, D. Lacoste, J. Pécréaux, J.-F. Joanny, J. Prost, and P. Bassereau, Phys. Rev. Lett. **102**, 038102 (2009).
[6] N. Gov, Phys. Rev. Lett. **93**, 268104 (2004).
[7] D. Lacoste and A. W. C. Lau, Europhys. Lett. **70**, 418 (2005).
[8] L.-L. Lin, N. Gov, and F. L. Brown, J. Chem. Phys. **124**, 074903 (2006).
[9] H.-Y. Chen and A. S. Mikhailov, Phys. Rev. E **81**, 031901 (2010).
[10] A. Alonso, H.-Y. Chen, M. Bär, and A. S. Mikhailov, Eur. Phys. J. Spec. Top. **191**, 131 (2010).
[11] B. L. de Groot and H. Grubmuller, Science **294**, 2353 (2001).
[12] G. Portella, T. Polupanow, F. Zocher, D. A. Boytsov, P. Pohl, U. Diederichsen, and B. L. de Groot, Biophys. J. **103**, 1698 (2012).
[13] N. Gō, Annu. Rev. Biophys. Bioeng. **12**, 183 (1983).
[14] M. M. Tirion, Phys. Rev. Lett. **77**, 1905 (1996).
[15] T. Haliloglu, I. Bahar, and B. Erman, Phys. Rev. Lett. **79**, 3090 (1997).
[16] A. R. Atilgan, S. R. Durell, R. L. Jernigan, M. C. Demirel, and O. Keskin, Biophys. J. **80**, 505 (2001).
[17] Y. Togashi and A. S. Mikhailov, Proc. Natl. Acad. Sci. U.S.A. **104**, 8697 (2007).
[18] H. Flechsig and A. S. Mikhailov, Proc. Natl. Acad. Sci. U.S.A. **107**, 20875 (2010).
[19] M. Düttmann, M. Mittnenzweig, Y. Togashi, T. Yanagida, and A. Mikhailov, PLoS ONE **7**, e45859 (2012).
[20] M. Düttmann, Y. Togashi, T. Yanagida, and A. Mikhailov, Biophys. J. **102**, 542 (2012).
[21] I. Bahar, A. R. Atilgan, and B. Erman, Folding Des. **2**, 173 (1997).
[22] A. Cressman, Y. Togashi, A. S. Mikhailov, and R. Kapral, Phys. Rev. E **77**, 050901 (2008).
[23] C. Echeverria, Y. Togashi, A. Mikhailov, and R. Kapral, Phys. Chem. Chem. Phys. **13**, 10527 (2011).
[24] I. R. Cooke, K. Kremer, and M. Deserno, Phys. Rev. E **72**, 011506 (2005).
[25] S. O. Nielsen, C. F. Lopez, G. Srinivas, and M. L. Klein, "Coarse grain models and the computer simulation of soft materials," J. Phys.: Condens. Matter **16**, R481 (2004).
[26] M. Venturoli, M. M. Sperotto, M. Kranenburg, and B. Smit, Phys. Rep. **437**, 1 (2006).
[27] J. C. Shillcock and R. Lipowsky, J. Chem. Phys. **117**, 5048 (2002).
[28] M. Laradji and P. S. Kumar, Phys. Rev. Lett. **93**, 198105 (2004).
[29] L. Gao, J. Shillcock, and R. Lipowsky, J. Chem. Phys. **126**, 015101 (2007).
[30] N. Malevanets and R. Kapral, J. Chem. Phys. **110**, 8605 (1999).
[31] N. Malevanets and R. Kapral, J. Chem. Phys. **112**, 7260 (2000).
[32] R. Kapral, Adv. Chem. Phys. **140**, 89 (2008).
[33] G. Gompper, T. Ihle, D. M. Kroll, and R. G. Winkler, Adv. Polym. Sci. **221**, 1 (2009).
[34] M.-J. Huang, R. Kapral, A. S. Mikhailov, and H.-Y. Chen, J. Chem. Phys. **137**, 055101 (2012).
[35] U. Schmidt, G. Guigas, and M. Weiss, Phys. Rev. Lett. **101**, 128104 (2008).
[36] F. J.-M. de Meyer, M. Venturoli, and B. Smit, Biophys. J. **95**, 1851 (2008).
[37] S. Li, X. Zhang, and W. Wang, Biophys. J. **98**, 2554 (2010).
[38] D. Morozova, G. Guigas, and M. Weiss, PLoS Comput. Biol. **7**, e1002067 (2011).
[39] K. Balali-Mood, P. J. Bond, and M. S. P. Sansom, Biochemistry **48**, 2135 (2009).
[40] M.-J. Huang, H.-Y. Chen, and A. S. Mikhailov, Eur. Phys. J. E **35**, 119 (2012).
[41] P. Maragakis and M. Karplus, J. Mol. Biol. **352**, 807 (2005).
[42] K. Okazaki, N. Koga, S. Takada, J. Onuchic, and P. Wolynes, Proc. Natl. Acad. Sci. U.S.A. **103**, 11844 (2006).
[43] K. Kremer and G. S. Grest, J. Chem. Phys. **92**, 5057 (1990).
[44] The hydrophobic machine particles are i = 1–4, 10–12, 54, 57–64.
[45] T. Ihle and D. M. Kroll, Phys. Rev. E **63**, 020201 (2001).
[46] T. Ihle and D. M. Kroll, Phys. Rev. E **67**, 066705 (2003).
[47] D. Reeves, T. Ursell, P. Sens, J. Kondev, and R. Phillips, Phys. Rev. E **78**, 041901 (2008).
[48] Using $\delta t = 10$ ps,[34] the mean closing time corresponds to 0.25μs, a value at the lower end for typical protein conformational changes (see R. B. Yirdaw and H. S. Mchaourab, Biophys. J. **103**, 1525 (2012)), so that even the time scales of such rapid protein conformational changes are longer than τ_c.
[49] H. Diamant, J. Phys. Soc. Jpn. **78**, 041002 (2009).
[50] P. G. Saffman and M. Delbrück, Proc. Natl. Acad. Sci. U.S.A. **72**, 3111 (1975).
[51] J. S. Guasto, K. A. Johnson, and J. P. Gollub, Phys. Rev. Lett. **105**, 168102 (2010).
[52] I. B. Bischofs, S. A. Safran, and U. S. Schwarz, Phys. Rev. E **69**, 021911 (2004).
[53] J. M. Schofield, P. Inder, and R. Kapral, J. Chem. Phys. **136**, 205101 (2012).
[54] J. Dursi, L. Groer, D. Gruner, C. Loken, S. Northrup, S. Ross, R. Sobie, and C. Yip, "High performance computing symposium (hpcs2010)," J. Phys.: Conf. Ser. **256**, 011001 (2010).